

## Electronic Supplementary Information

# Ni-Mo nitride synthesized via mild plasma for efficient alkaline hydrogen evolution electrocatalysis

Yunpeng Wei,<sup>a</sup> Lingya Yi,<sup>a</sup> Siyue Zhang,<sup>b</sup> Chengsheng Ni,<sup>\*c</sup> Xinghong Cai,<sup>\*a</sup> Wei Sun,<sup>\*b</sup> and Weihua Hu<sup>\*a</sup>

<sup>a</sup>. School of Materials and Energy, Chongqing Key Laboratory for Advanced Materials and Technologies of Clean Energies, Southwest University, Chongqing 400715, P. R. China. Email: [cjh112233@email.swu.edu.cn](mailto:cjh112233@email.swu.edu.cn); [whhu@swu.edu.cn](mailto:whhu@swu.edu.cn)

<sup>b</sup>. Key Laboratory of Laser Technology and Optoelectronic Functional Materials of Hainan Province, Key Laboratory of Functional Materials and Photoelectrochemistry of Haikou, College of Chemistry and Chemical Engineering, Hainan Normal University, Haikou 571158, P. R. China. Email: [sunwei@hainnu.edu.cn](mailto:sunwei@hainnu.edu.cn)

<sup>c</sup>. College of Resources and Environment, Southwest University, Chongqing 400715, P. R. China. Email: [nichengsheg@swu.edu.cn](mailto:nichengsheg@swu.edu.cn)

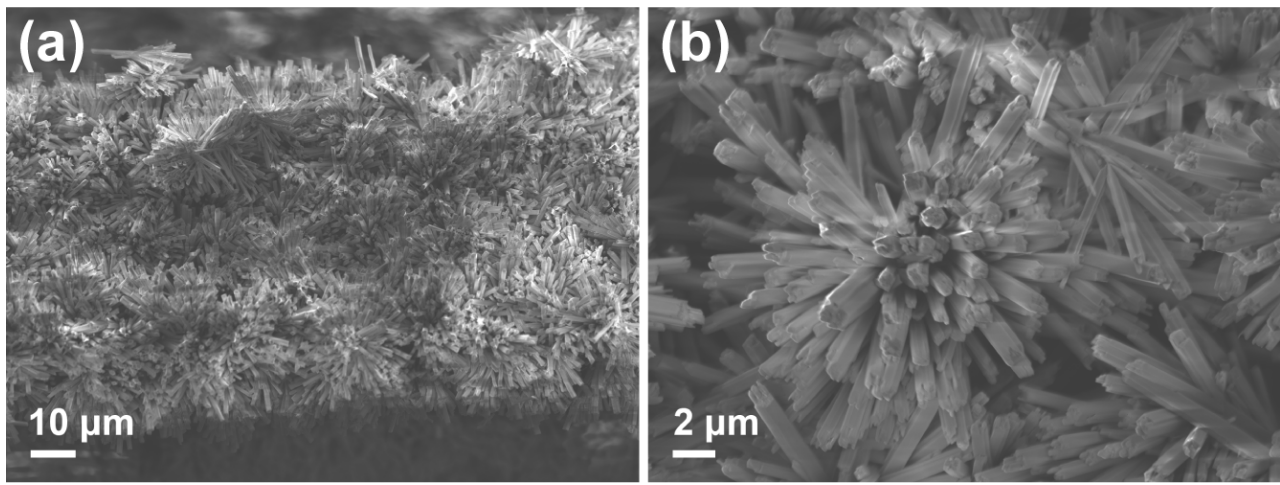


**Fig. S1.** SEM images of NMO/NF. Due to the poor conductivity of this crystalline oxide hydrate precursor, the SEM images show bright stripes due to local electron accumulation.

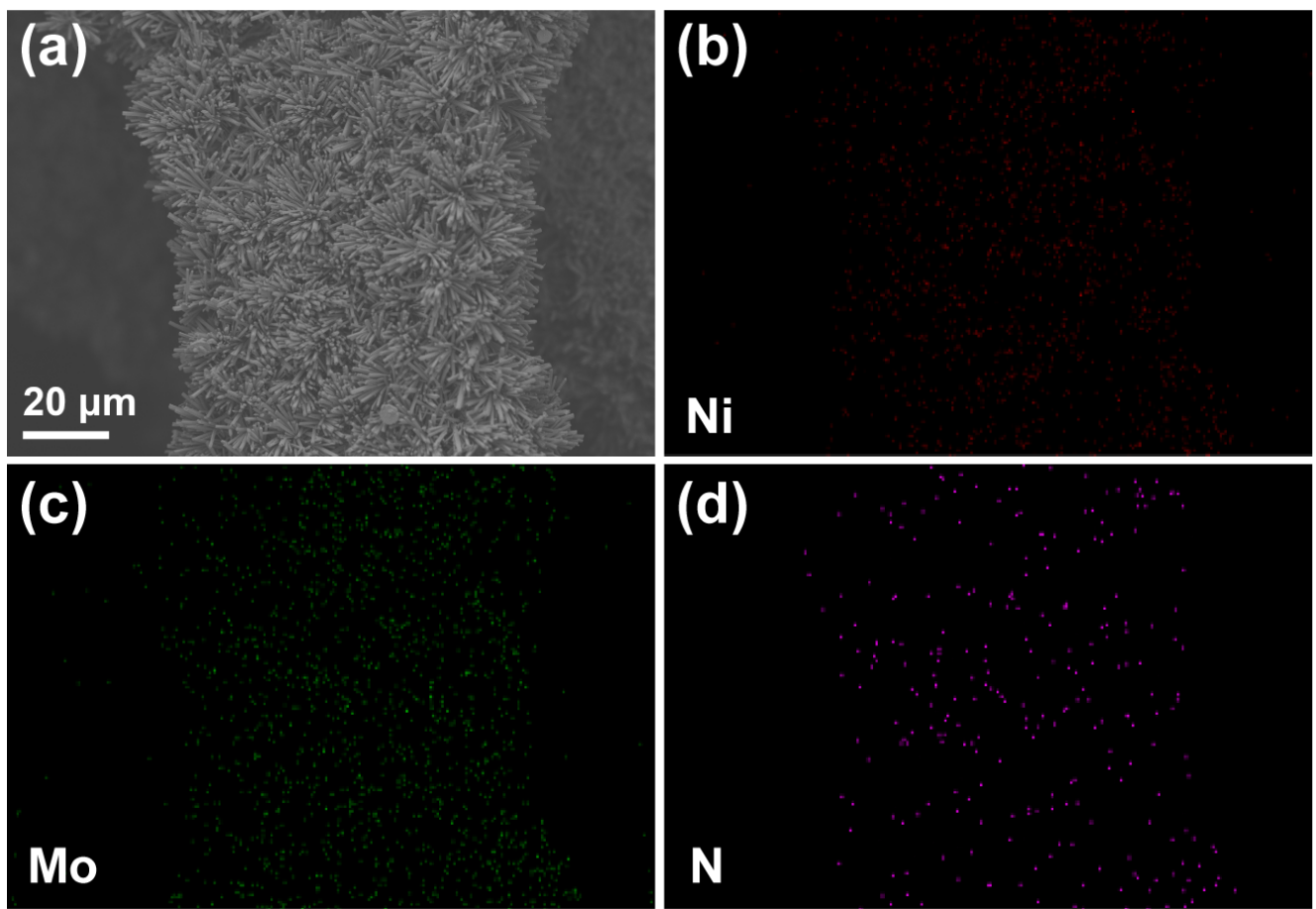


**Fig. S2.** (a) SEM image of NMN/NF and corresponding EDS elemental mappings of Ni (b), Mo (c) and N (d).

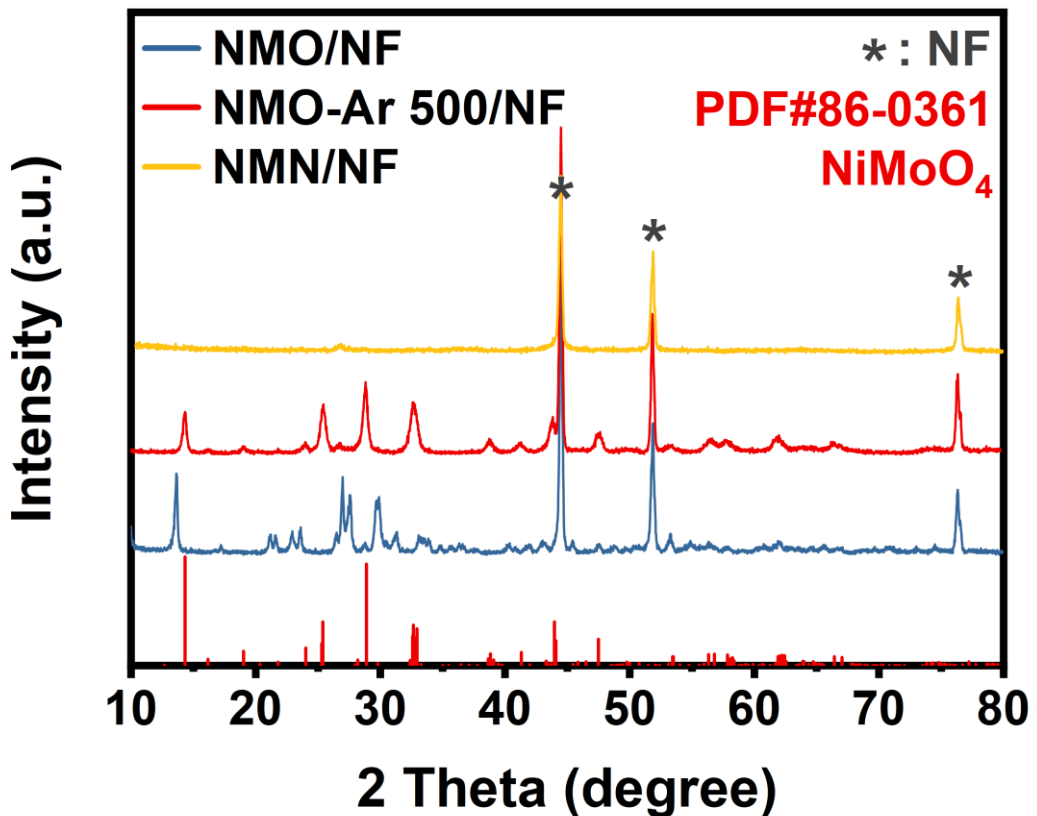


**Fig. S3.** XRD patterns of NMO/NF, NMO/NF annealed at 500 °C and NMN/NF. The Ni-Mo oxide hydrate phase ( $\text{NiMoO}_4 \cdot x\text{H}_2\text{O}$ , PDF no. 13-0128) in NMO/NF was converted to  $\text{NiMoO}_4/\text{NF}$  (PDF no. 86-0361) after annealing at 500 °C.

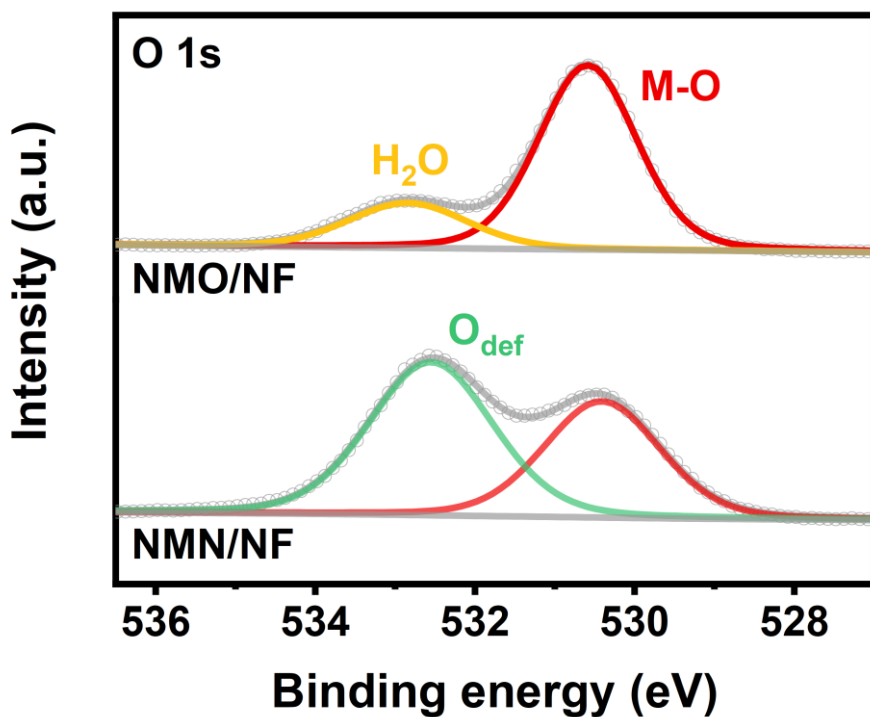


**Fig. S4.** O 1s XPS spectra of NMO/NF and NMN/NF.

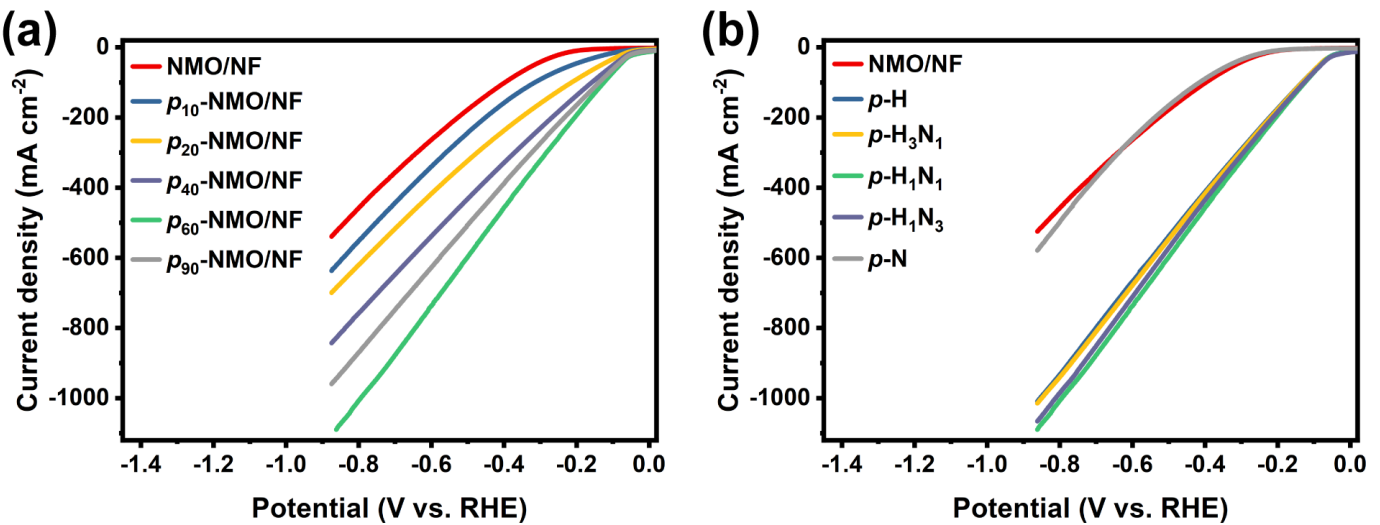


**Fig. S5.** Optimization of  $\text{H}_2/\text{N}_2$  plasma duration and  $\text{H}_2/\text{N}_2$  ratio in terms of HER activity (Without iR correction). (a) LSV curves of NMN/NF with different plasma processing time. (b) LSV curves of NMN/NF with different ratio of  $\text{H}_2$  and  $\text{N}_2$ .  $p\text{-H}$  and  $p\text{-N}$  sample are obtained with pure  $\text{H}_2$  and  $\text{N}_2$  plasma, respectively. For  $p\text{-H}_3\text{N}_1$ ,  $p\text{-H}_1\text{N}_1$ , and  $p\text{-H}_1\text{N}_3$ , the  $\text{H}_2/\text{N}_2$  ratios are 3:1, 1:1 and 1:3, respectively. The whole pressure remains 30 Pa for all samples.

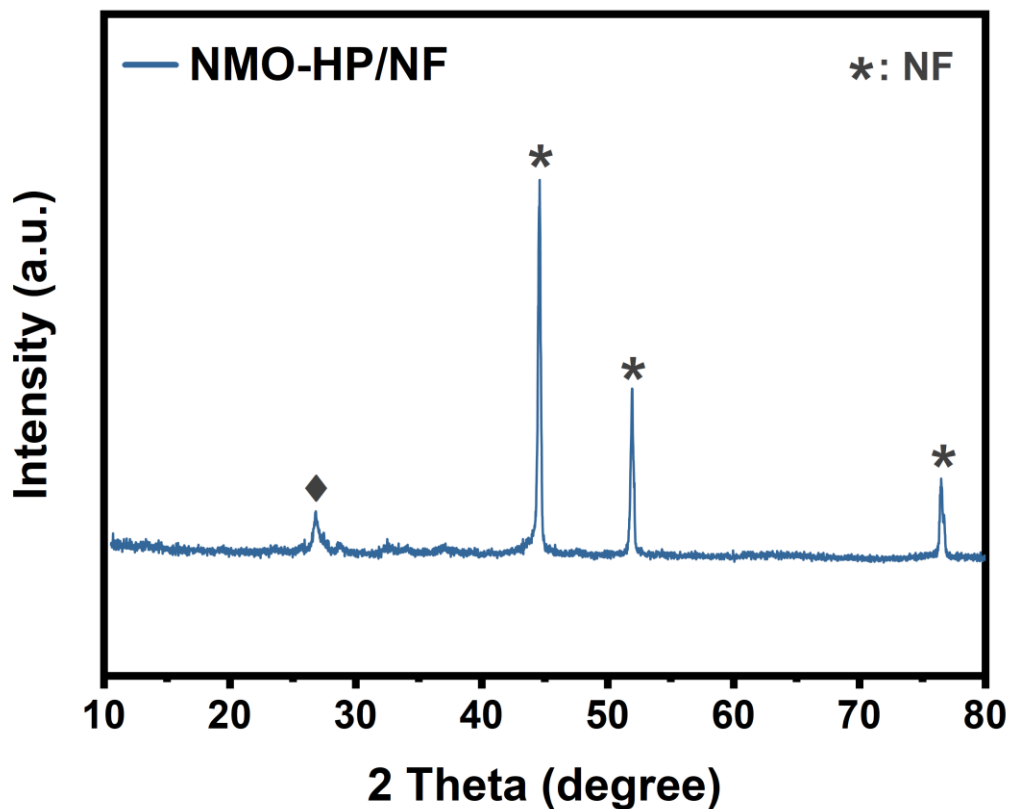


**Fig. S6.** XRD pattern of NMO/NF after processed in  $\text{H}_2$  plasma.

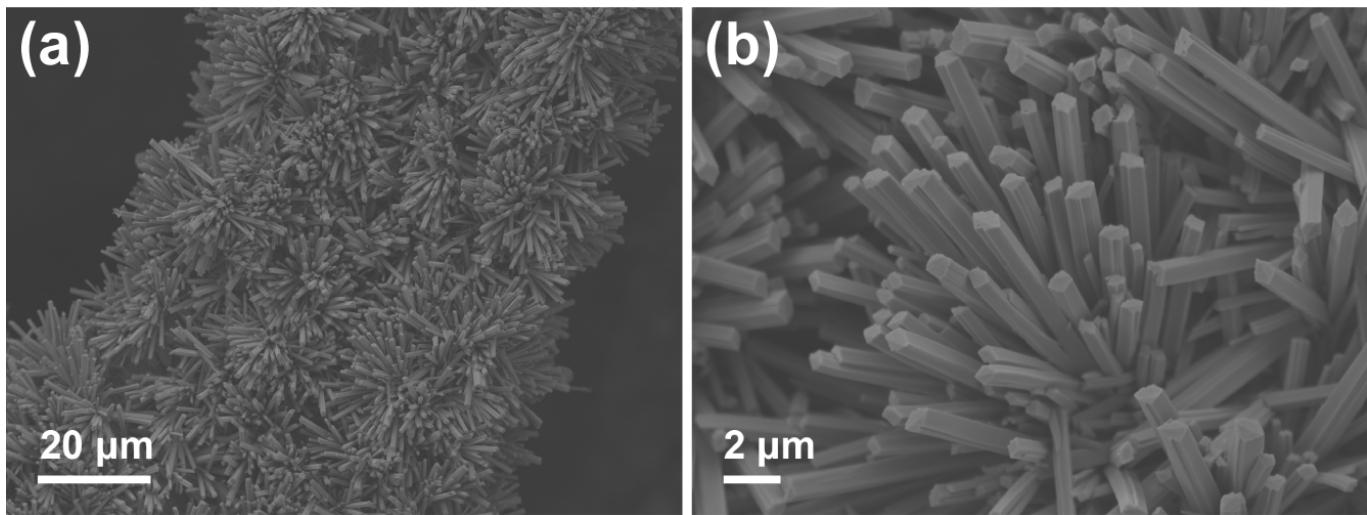


**Fig. S7.** Low-resolution (a) and high-resolution (b) SEM images of NMO/NF after processed in H<sub>2</sub> plasma.

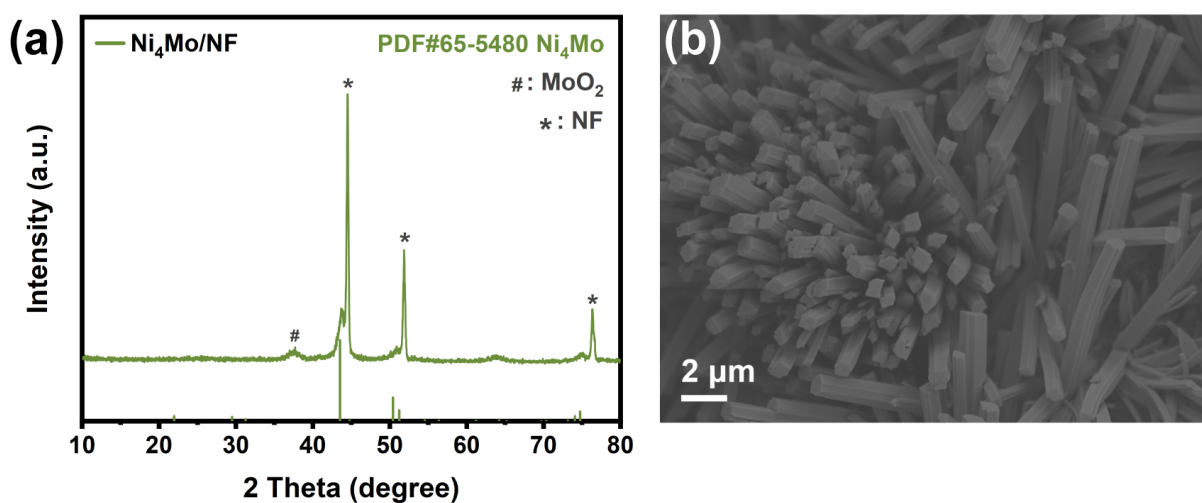


**Fig. S8.** (a) XRD pattern and (b) SEM image of  $\text{Ni}_4\text{Mo}/\text{NF}$ . XRD pattern suggests that NMO precursor was transformed into  $\text{Ni}_4\text{Mo}$  alloy (PDF#65-5480) and a small amount of  $\text{MoO}_2$  remains after annealing in H<sub>2</sub>/Ar atmosphere at 600°C. SEM image shows that  $\text{Ni}_4\text{Mo}/\text{NF}$  retains the nanorod morphology of NMO/NF precursor.

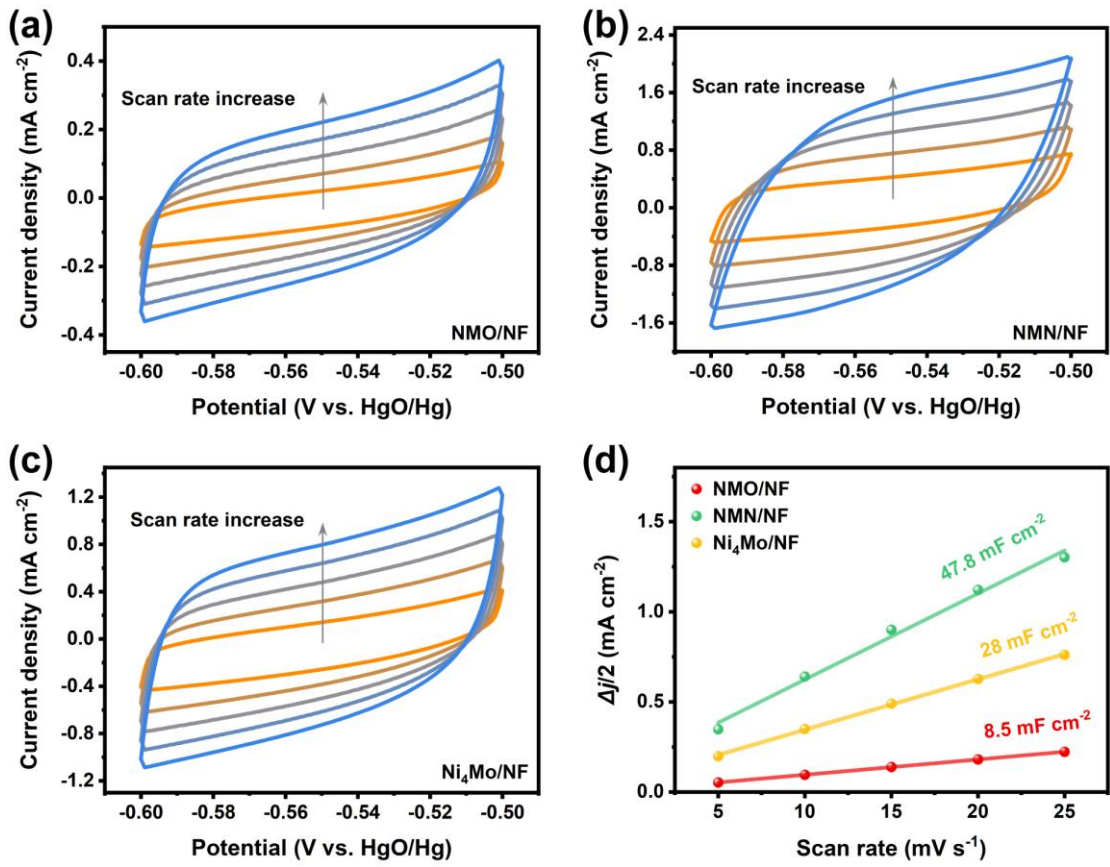


**Fig. S9.** (a-c) CV curves of NMO/NF (a), NMN/NF (b) and  $\text{Ni}_4\text{Mo}/\text{NF}$  (c) with different scan rates at non-Faradaic potential range; (d) corresponding double-layer capacitance ( $C_{\text{dl}}$ ).

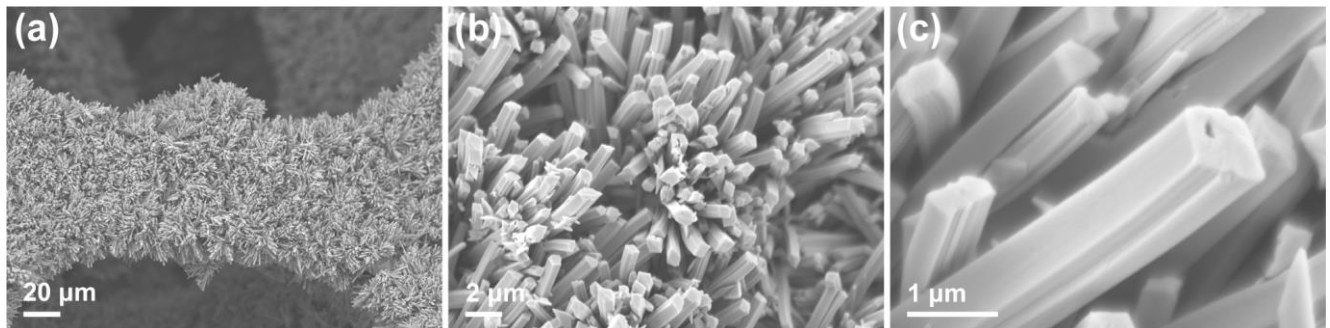


**Fig. S10.** SEM images of NMN/NF after HER stability test (50 h at  $100 \text{ mA cm}^{-2}$ ).

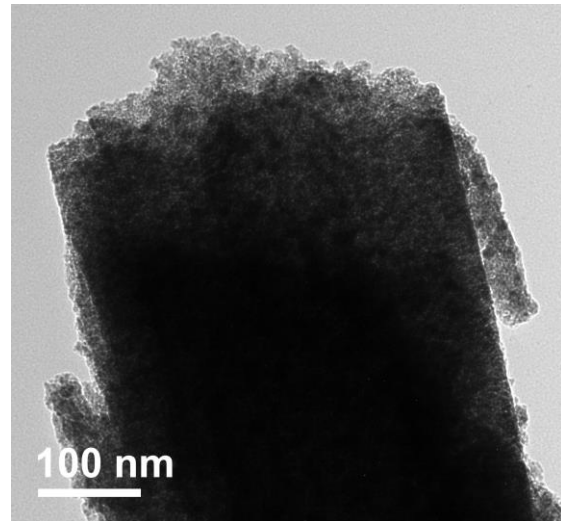


**Fig. S11.** TEM image of NMN/NF after HER stability test (50 h at 100 mA cm<sup>-2</sup>).

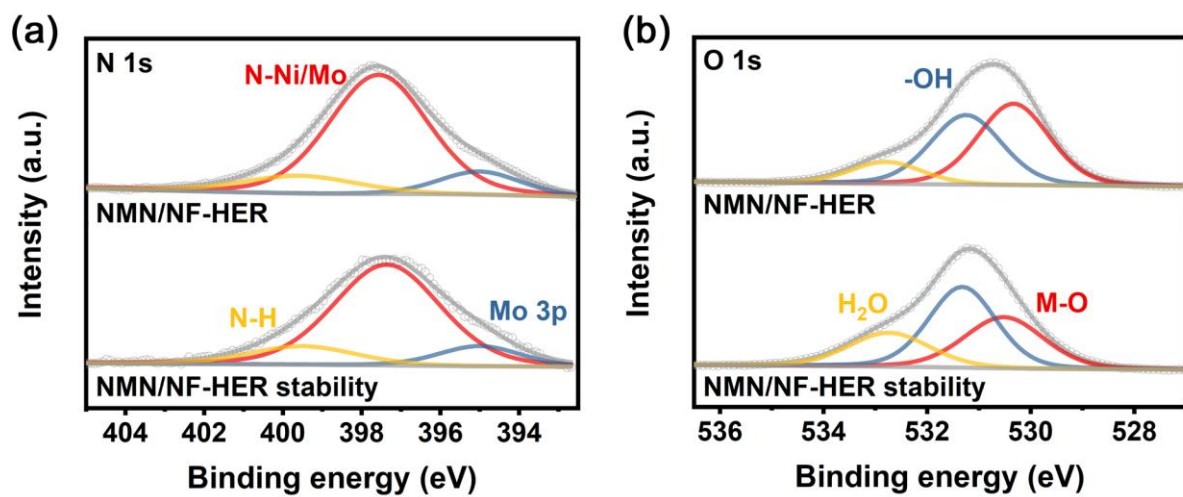


**Fig. S12.** XPS spectra of NMN/NF after HER and long-term HER stability test: (a) N 1s and (b) O 1s.

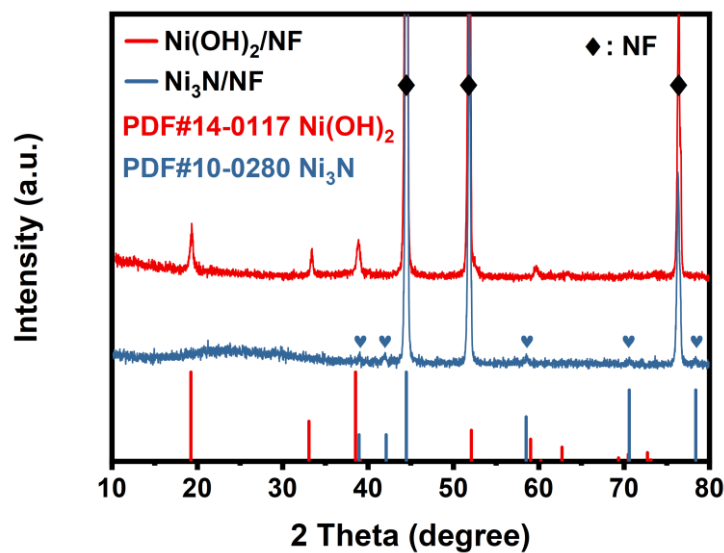


**Fig. S13.** XRD pattern of Ni(OH)<sub>2</sub>/NF before and after H<sub>2</sub> /N<sub>2</sub> plasma treatment (denoted as Ni<sub>3</sub>N/NF).

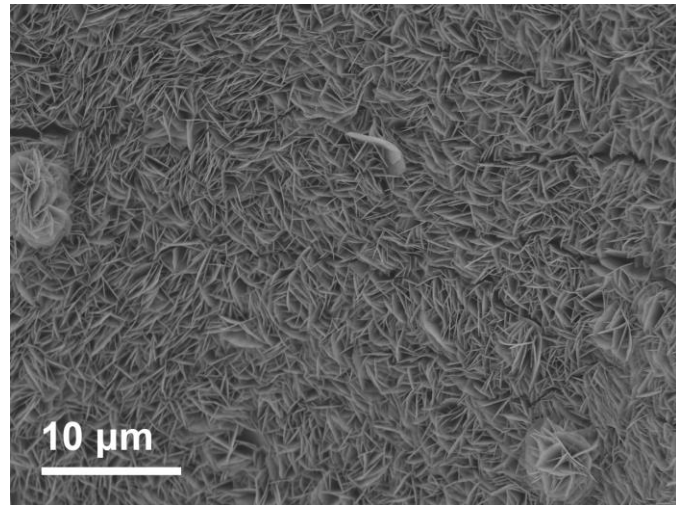


**Fig. S14.** SEM image of  $\text{Ni}(\text{OH})_2/\text{NF}$ .

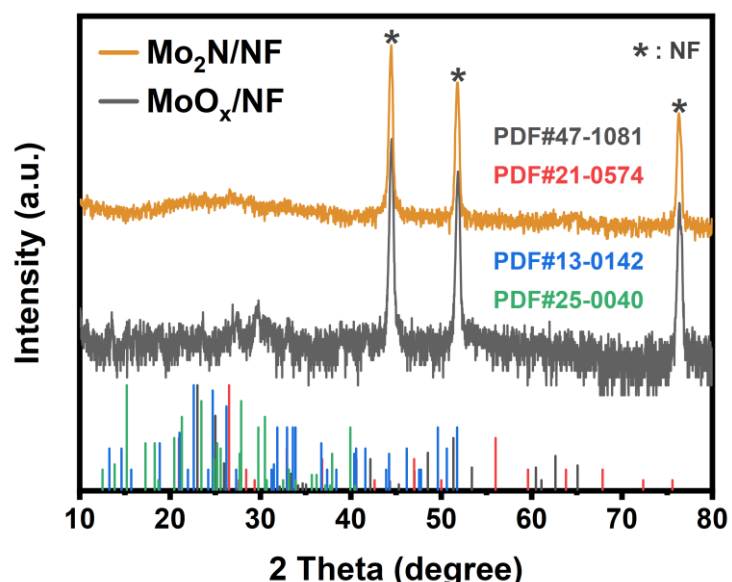


**Fig. S15.** XRD pattern of  $\text{MoO}_x/\text{NF}$  before and after  $\text{H}_2/\text{N}_2$  plasma treatment (denoted as  $\text{Mo}_2\text{N}/\text{NF}$ ).

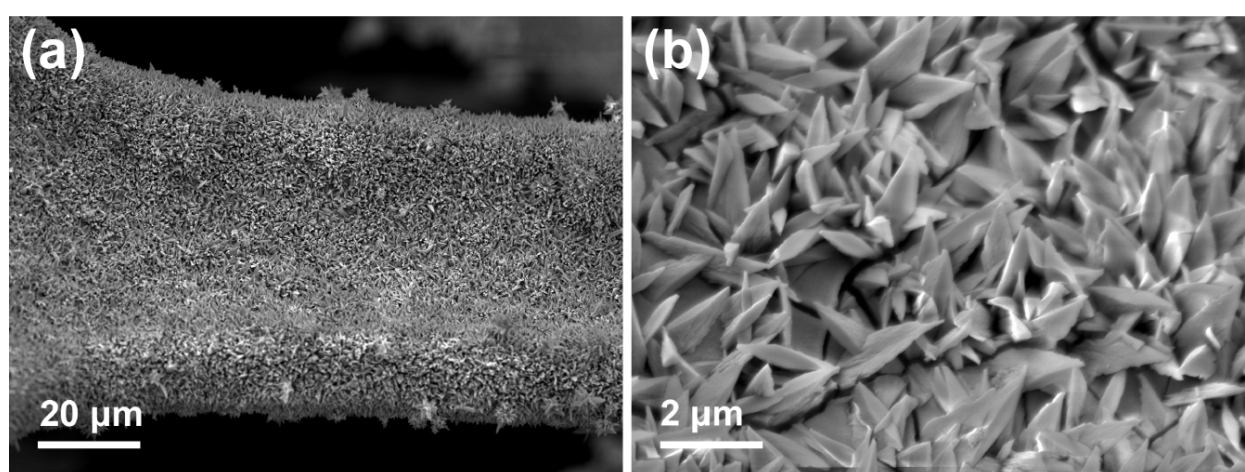


**Fig. S16.** Low-(a) and high-(b) resolution SEM images of  $\text{MoO}_x/\text{NF}$ .

**Table S1.** Comparison of the catalytic HER performance between our *p*-NMO/NF and non-noble metal nitride-based electrocatalysts reported in alkaline condition.

Catalyst	Substrate	$\eta_{100}$ (mV)	Tafel slope (mV dec <sup>-1</sup> )	Electrolyte	Ref.
<b>NMN/NF</b>	NF <sup>a</sup>	66	38	1.0 M KOH	This work
<b>Ni<sub>4</sub>Mo/NF</b>	NF	99	66.8	1.0 M KOH	This work
<b>Ni-MoN</b>	CF <sup>b</sup>	61	35.5	1.0 M KOH	[1]
<b>Ni<sub>3</sub>N-NiMoN/CC</b>	CC <sup>c</sup>	74	40	1.0 M KOH	[2]
<b>Ni<sub>3</sub>N@NiMoN<sub>x</sub>/NF</b>	NF	78	55	1.0 M KOH	[3]
<b>NiMoN/Ni<sub>3</sub>N-12</b>	NF	93	49	1.0 M KOH	[4]
<b>Ni<sub>3</sub>N@C/NF</b>	NF	95	60	1.0 M KOH	[5]
<b>Ni<sub>3</sub>N@2M-MoS<sub>2</sub></b>	NF	97	43.2	1.0 M KOH	[6]
<b>P-Mo-Ni(OH)<sub>2</sub> NSAs</b>	NF	98	80	1.0 M KOH	[7]
<b>(Fe<sub>0.74</sub>Co<sub>0.26</sub>)<sub>2</sub>P/Ni<sub>3</sub>N</b>	NF	113	31.8	1.0 M KOH	[8]
<b>Co/MoN</b>	NF	132	77.5	1.0 M KOH	[9]
<b>NiMoN/NiN</b>	NF	136	70	1.0 M KOH	[10]
<b>P-MoP/Mo<sub>2</sub>N</b>	NF	137	78	1.0 M KOH	[11]
<b>Ni<sub>3</sub>N NCs</b>	GC <sup>d</sup>	142	49	1.0 M KOH	[12]
<b>2D meso-Mo<sub>2</sub>C/Mo<sub>2</sub>N</b>	GC	164	44.1	1.0 M KOH	[13]
<b>V-Ni<sub>3</sub>N/NF</b>	NF	172	45	1.0 M KOH	[14]
<b>cp-Ni<sub>3</sub>N</b>	Ni plate	183	64	1.0 M NaOH	[15]
<b>NiPN/Ni/CC-CNT<sup>2</sup></b>	CC	186	50	1.0 M KOH	[16]
<b>Ni<sub>3</sub>N-VN/NF</b>	NF	218	37	1.0 M KOH	[17]
<b>N10V7M3</b>	NF	253	94	1.0 M KOH	[18]

Notes:  $\eta_{100}$  means the overpotentials at current density of 100 mA cm<sup>-2</sup>; <sup>a</sup> NF: nickel foam, <sup>b</sup> CF: copper foam, <sup>c</sup> CC: carbon cloth, <sup>d</sup> GC: glassy carbon.

## Reference

- [1] L. Wu, F. Zhang, S. Song, M. Ning, Q. Zhu, J. Zhou, G. Gao, Z. Chen, Q. Zhou, X. Xing, T. Tong, Y. Yao, J. Bao, L. Yu, S. Chen, Z. Ren, *Adv. Mater.* **2022**, *34*, e2201774.
- [2] J. Zeng, W. Chen, G. Zhang, L. Yu, L. Zhong, Y. Liu, S. Zhao, Y. Qiu, *ACS Applied Nano Materials* **2022**, *5*, 7321.
- [3] P. Chen, D. Feng, K. Li, Y. Tong, *Dalton Transactions* **2022**, *51*, 16990.
- [4] W. Hua, H. Sun, H. Liu, Y. Li, J.-G. Wang, *Appl. Surf. Sci.* **2021**, *540*, 148407.
- [5] B. Wang, M. Lu, D. Chen, Q. Zhang, W. Wang, Y. Kang, Z. Fang, G. Pang, S. Feng, *J. Mater. Chem. A* **2021**, *9*, 13562.
- [6] T. Wu, E. Song, S. Zhang, M. Luo, C. Zhao, W. Zhao, J. Liu, F. Huang, *Adv. Mater.* **2022**, *34*, e2108505.
- [7] W. Zhang, Y. Tang, L. Yu, X.-Y. Yu, *Appl. Catal. B* **2020**, *260*, 118154.
- [8] W. Ma, D. Li, L. Liao, H. Zhou, F. Zhang, X. Zhou, Y. Mo, F. Yu, *Small* **2023**, *19*, e2207082.
- [9] J. Sun, W. Xu, C. Lv, L. Zhang, M. Shakouri, Y. Peng, Q. Wang, X. Yang, D. Yuan, M. Huang, Y. Hu, D. Yang, L. Zhang, *Appl. Catal. B* **2021**, *286*, 119882.
- [10] B. Wang, L. Guo, J. Zhang, Y. Qiao, M. He, Q. Jiang, Y. Zhao, X. Shi, F. Zhang, *Small* **2022**, *18*, e2201927.
- [11] Y. Gu, A. Wu, Y. Jiao, H. Zheng, X. Wang, Y. Xie, L. Wang, C. Tian, H. Fu, *Angew. Chem. Int. Ed.* **2021**, *60*, 6673.
- [12] G. S. Shanker, S. Ogale, *ACS Appl. Energy Mater.* **2021**, *4*, 2165.
- [13] S. Li, Z. Zhao, T. Ma, P. Pachfule, A. Thomas, *Angew. Chem. Int. Ed.* **2022**, *61*, e202112298.
- [14] R.-Q. Li, Q. Liu, Y. Zhou, M. Lu, J. Hou, K. Qu, Y. Zhu, O. Fontaine, *J. Mater. Chem. A* **2021**, *9*, 4159.
- [15] B. Ouyang, Y. Zhang, X. Wang, Y. Deng, F. Liu, Z. Fang, R. S. Rawat, E. Kan, *Small* **2022**, *18*, e2204634.
- [16] M. Liu, E. Wang, Z. Zhao, *ACS Applied Nano Materials* **2022**, *5*, 5335.
- [17] H. Yan, Y. Xie, A. Wu, Z. Cai, L. Wang, C. Tian, X. Zhang, H. Fu, *Adv. Mater.* **2019**, *31*, e1901174.
- [18] N. Sinha, P. Roy, *Inorg. Chem.* **2023**, *62*, 3349.